The Ocular Surface 18 (2020) 545–553

Contents lists available at ScienceDirect

The Ocular Surface

journal homepage: www.elsevier.com/locate/jtos

Clinical Practice

# Interactions of polar lipids with cholesteryl ester multilayers elucidate tear film lipid layer structure

Riku O. Paananen[a,*], Tuomo Viitaja[a,b], Agnieszka Olżyńska[c], Filip S. Ekholm[b], Jukka Moilanen[a], Lukasz Cwiklik[c]

[a] Helsinki Eye Lab, Ophthalmology, University of Helsinki and Helsinki University Hospital, Haartmaninkatu 8, FI-00290, Helsinki, Finland
[b] Department of Chemistry, University of Helsinki, P.O. Box 55, FI-00014, Helsinki, Finland
[c] J. Heyrovský Institute of Physical Chemistry, Czech Academy of Sciences, Dolejškova 3, 182 23, Prague, Czech Republic

ARTICLE INFO

*Keywords:*
Cholesteryl ester
Dry eye
Evaporation
Lipid multilayer
*O*-Acyl-ω-hydroxy fatty acid
Phospholipid
Tear film lipid layer

ABSTRACT

*Purpose:* The tear film lipid layer (TFLL) covers the tear film, stabilizing it and providing a protective barrier against the environment. The TFLL is divided into polar and non-polar sublayers, but the interplay between lipid classes in these sublayers and the structure-function relationship of the TFLL remains poorly characterized. This study aims to provide insight into TFLL function by elucidating the interactions between polar and non-polar TFLL lipids at the molecular level.

*Methods:* Mixed films of polar *O*-acyl-ω-hydroxy fatty acids (OAHFA) or phospholipids and non-polar cholesteryl esters (CE) were used as a model of the TFLL. The organization of the films was studied by using a combination of Brewster angle and fluorescence microscopy in a Langmuir trough system. In addition, the evaporation resistance of the lipid films was evaluated.

*Results:* Phospholipids and OAHFAs induced the formation of a stable multilamellar CE film. The formation of this film was driven by the interdigitation of acyl chains between the monolayer of polar lipids and the CE multilayer lamellae. Surprisingly, the multilayer structure was destabilized by both low and high concentrations of polar lipids. In addition, the CE multilayer was no more effective in resisting the evaporation of water than a polar lipid monolayer.

*Conclusions:* Formation of multilamellar films by major tear film lipids suggest that the TFLL may have a similar structure. Moreover, in contrast to the current understanding, polar TFLL lipids may not mainly act by stabilizing the non-polar TFLL sublayer, but through a direct evaporation resistant effect.

## 1. Introduction

The surface of the eye is covered by the tear film, a layer of aqueous tear fluid that forms a smooth refractive surface and protects the underlying epithelial cells. The aqueous tear film is covered by the tear film lipid layer (TFLL), a thin, oily layer that acts as a barrier between the aqueous tear fluid and the environment and is considered to prevents excess evaporation of water from the tear film [1]. Impaired TFLL evaporation resistance leads to hyperosmolarity of the tear fluid, which causes an inflammatory response and damages the ocular surface cells. This results in symptoms such as pain and blurring of vision, and further destabilizes the tear film, potentially leading to development of dry eye syndrome (DES) [1]. In severe cases of DES, the loss of lubrication by the tear film can lead to corneal ulceration and scarring [2].

Most cases of DES are associated with dysfunctional Meibomian glands that produce the TFLL lipids [3,4]. Dysfunction of the Meibomian glands causes changes in TFLL lipid quality and quantity [5,6], which is likely to impair the ability of the TFLL to resist evaporation. This link between TFLL composition and function has been suggested by recent animal studies, where changes in tear film lipid composition, caused by mutations of genes involved in Meibomian lipid synthesis (*Elovl1*, *Elovl3, or Cyp4f39*), led to a severe dry eye phenotype [7–9]. However, it is still unclear what kind of compositional changes are associated with dry eye in humans, and various studies have reported changes in different lipid classes related to dry eye [10–14]. Further, the functional consequences of these compositional changes are speculative, since the molecular mechanisms of TFLL evaporation resistance remain poorly understood. The TFLL can be divided into two parts: a monolayer of polar lipids, which resides at the surface of the aqueous tear fluid, and a thicker layer of non-polar lipids that cover the polar

* Corresponding author.Haartmaninkatu 8, FI-00290, Helsinki, Finland.
*E-mail address:* riku.o.paananen@helsinki.fi (R.O. Paananen).

https://doi.org/10.1016/j.jtos.2020.06.001
Received 23 March 2020; Received in revised form 31 May 2020; Accepted 4 June 2020

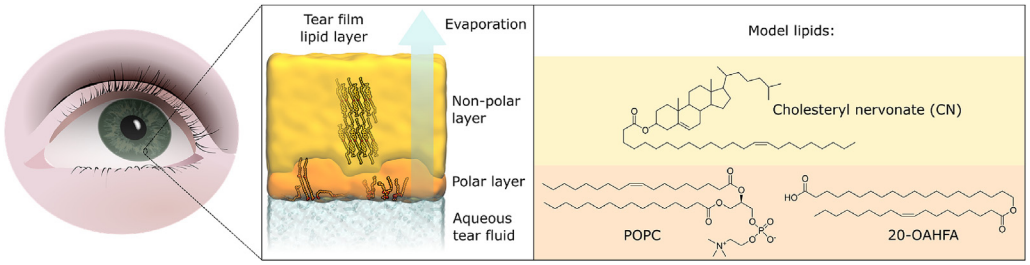


**Fig. 1.** A model of the tear film lipid layer (TFLL). **Left:** A schematic representation of the overall organization of the TFLL. **Right:** Model lipids corresponding to the non-polar and polar layers of the TFLL.

sublayer (Fig. 1) [15]. This general structure aside, no consensus exists on TFLL organization and several different models have been proposed [12,16–20].

To shed light on this matter, we studied the organization and biophysical properties of TFLL-mimicking mixtures of polar and non-polar tear film lipids with Langmuir trough-based techniques. The main polar lipids in the tear film are phospholipids and *O*-acyl-ω-hydroxy fatty acids (OAHFAs), whereas cholesteryl esters (CEs) and wax esters (WEs) are the most abundant non-polar lipids [10,21,22]. In this study, we used 1-palmitoyl-2-oleoyl-*sn*-glycero-3-phosphocholine (POPC) and (*O*-oleoyl)-ω-hydroxy arachidic acid (20-OAHFA) to represent polar TFLL lipids, while the non-polar TFLL lipids were represented by cholesteryl nervonate (CN) (Fig. 1). In order to understand the interplay between polar and non-polar lipids in the TFLL, we varied their ratios and explored the effects on organization and related biophysical properties of the film. In addition, the lipid films were imaged using both Brewster angle- (BAM) and fluorescence microscopy (FM), allowing visualization of both the non-polar and polar layers of the multi-layered films.

Our aim was to investigate three key aspects of TFLL structure: the role of polar lipids in TFLL organization, the structure of the non-polar layer of TFLL, and origin of TFLL evaporation resistance.

First, polar lipids are widely considered to be of key importance in maintaining TFLL structure and function by acting as a surfactant between the aqueous tear film and the non-polar lipid layer [15]. However, the role of different polar lipid classes in TFLL organization is currently unknown [23], resulting in continuous debate over the importance of phospholipids [19] versus OAHFAs [21]. Herein, we studied the behaviour of both polar lipids and found that they induce the formation of an overlying CN multilayer at low surface concentrations. However, at higher surface concentrations of polar lipids the multilayer was destabilized, and only films containing OAHFAs resisted evaporation.

Second, the structure within the non-polar region of the TFLL is not well documented. X-ray diffraction and infrared spectroscopy studies have shown that Meibomian lipids are partially ordered at physiological conditions and form multilamellar structures [24–26], but it is unclear how these lamellae are organized in the TFLL. Some have suggested that TFLL has a uniform multilamellar structure [12,16], while others have argued for a disordered structure with dispersed solid crystallites [17,20]. In this study, we address this topic and demonstrate how films including CN organize into multilamellar structures with discrete lamellae. Furthermore, we provide molecular level insight into the underlying factors *i.e.* the importance of interdigitation between the polar and non-polar layers.

Third, the thickness of the non-polar layer of the TFLL has been considered to be important in determining the evaporation resistance of the TFLL [27,28]. However, this idea has been recently challenged [29], and the internal structure within the TFLL responsible for evaporation resistance remains unknown. We therefore investigated whether the formation of non-polar CN multilayers provide increased evaporation resistance, compared to a monolayer of polar lipids, but found no detectable increase in evaporation resistance compared to phospholipids or OAHFAs alone. In total, this study provides insight into the multilamellar organization of CEs at the air-water interface as well as the interplay of polar and non-polar lipids in such films.

## 2. Material and methods

### 2.1. Materials

1-palmitoyl-2-oleoyl-*sn*-glycero-3-phosphocholine (POPC) was obtained from Avanti Polar Lipids (Alabaster, AL) and cholesteryl nervonate (CN) was purchased from Nu-Chek Prep (Elysian, MN). (*O*-oleoyl)-ω-hydroxy arachidic acid (20-OAHFA) was synthesised as described previously [30]. Fluorescent 1,2-dioleoyl-*sn*-glycero-3-phosphoethanolamine (DOPE) labeled with Atto 633 (Atto633-DOPE) was obtained from ATTO-TEC (Siegen, Germany). All the lipids were dissolved in chloroform of spectroscopic grade and stored at −20 °C until used. Milli-Q water was used as the sub-phase in the experiments including phospholipids. For OAHFA-containing mixtures, phosphate-buffered saline (PBS) was used as the subphase, to achieve the natural degree of ionization of the OAHFA carboxylic acid groups.

### 2.2. Brewster angle microscopy and surface potential

Lipids in chloroform solution were added to the air-water interface of a KSV Minitrough (KSV, Espoo, Finland) with Hamilton microsyringe. Trough temperature was maintained at 35 °C during the experiments using a Lauda ECO E4 thermostat (Lauda, Germany). After allowing for the chloroform to evaporate for 3 min, the film was compressed at a constant rate of 10 mm/min. Surface pressure was measured using a Wilhelmy plate, surface potential was measured using KSV SPOT (Espoo, Finland), and Brewster angle microscopy images were captured using KSV NIMA microBAM (Espoo, Finland). All the measurements were performed within an acrylic box (volume 80 l). Dry air was passed through an ODS-3P ozone destruct unit (Ozone solutions, Hull, Iowa) and into the acrylic box at a rate of 76 l/min to maintain an ozone-free atmosphere and prevent oxidation of unsaturated lipids during the experiments.

### 2.3. Fluorescence microscopy

Lipid mixtures, where 0.2% of the polar lipid (POPC or 20-OAHFA) was replaced with fluorescent Atto633-DOPE, were prepared in chloroform. Lipid solution was spread by depositing small droplets with Hamilton microsyringe over a subphase filling stainless steel trough with poly (tetrafluoroethylene) (PTFE) edges and a quartz-glass window (μTrough XS, Kibron; Helsinki, Finland). Chloroform was allowed to evaporate for 8 min, and the film was compressed with the symmetrical movement of two barriers at a constant rate of 5 mm/min. Surface pressure was measured using a surface pressure sensor (KBN 315; Kibron) with a DyneProbe. During compression the film was imaged using an inverted fluorescence microscope (Olympus, Hamburg, Germany) equipped with UPlanSApo 10 × objective (NA 0.4, WD 3.1 mm, Olympus). The fluorescent probe was excited with a Mercury lamp and the intensity of the light was controlled with neutral density

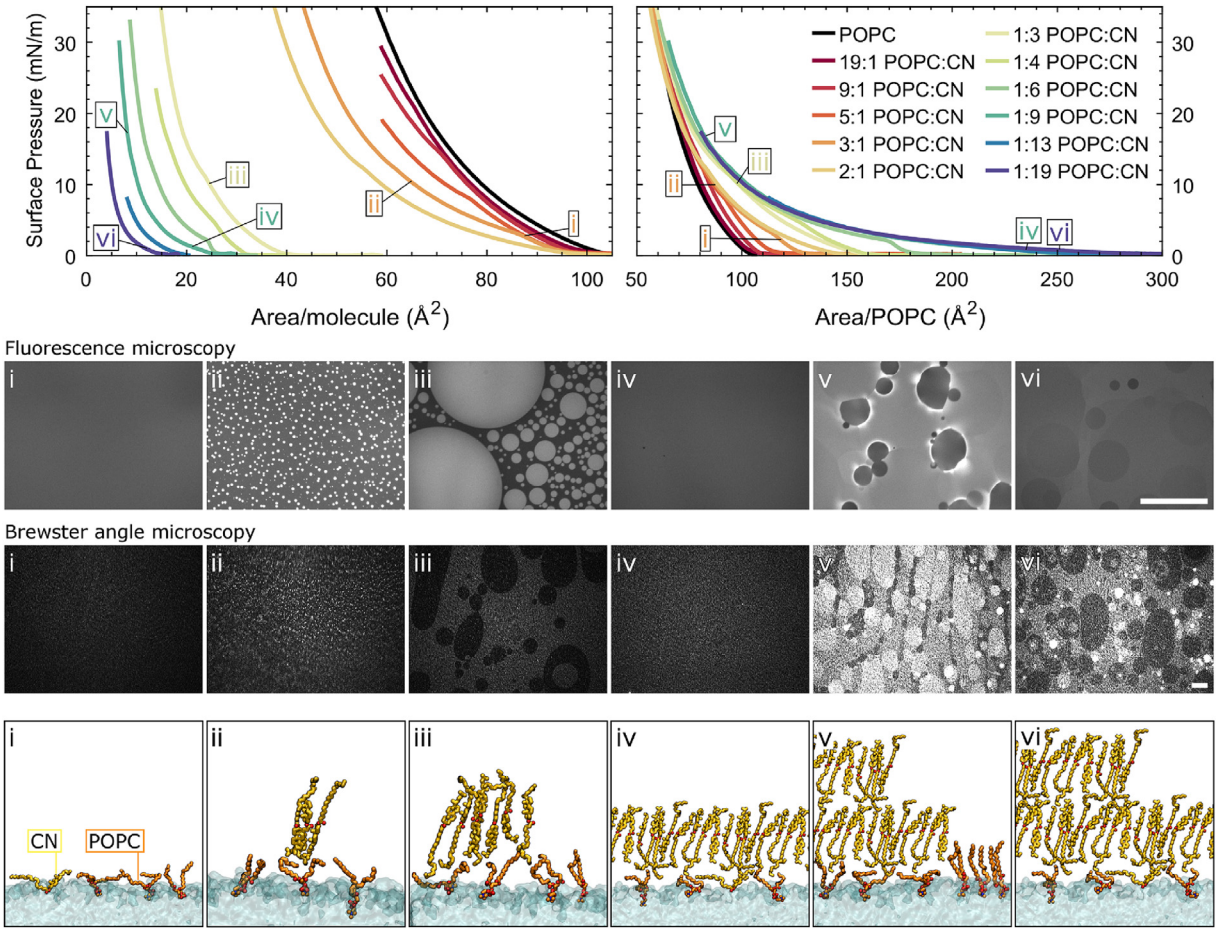


**Fig. 2.** Organization of mixed multilayers of POPC and CN. Representative surface pressure isotherms of POPC:CN mixtures with the corresponding FM and BAM images, as well as a schematic representation of the film structure at different film compositions and surface pressures (i–vi). The measurements were repeated at least twice and were found to be repeatable within 1.5 mN/m. The isotherms are presented both relative to the total number of molecules (left) and to the number of POPC molecules (right). Scale bars represent 300 μm.

filter. Dichroic cube Cy5-A-Basic-000 (Semrock) with 630/38 and 694/44 as a single-band excitation and emission filters, respectively, was inserted in the light pathway. Emission light was detected with a CCD camera (Olympus, Tokyo, Japan). All the measurements were performed at 35 °C, controlled with a temperature control plate connected to a water-circulating thermostat (Julabo F12-EC, Julabo, Seelbach, Germany), within an acrylic box to prevent subphase evaporation and contamination by dust.

### 2.4. Image analysis

All image analysis was performed with Matlab R2017a. Brewster angle microscopy images were segmented into different intensity regions by performing the following steps: First, uneven illumination was corrected by smoothing the images using a gaussian filter with a standard deviation of 100 pixels and the original image was divided by the smoothed image to normalize the local image intensity. Second, the normalized image was cropped to exclude non-focused areas of the image caused by the tilted orientation of the objective in BAM. Only the regions within 200 pixels from the intensity maximum of the smoothed image in the Y-direction were included in the analysis. Third, the normalized image was smoothed using a circular averaging filter with 5-pixel radius. Fourth, the images were segmented using multilevel thresholding with Otsu's method [31]. The discriminant criterion η was calculated for 1 to 3 thresholds for each image and compared to the discriminant criterion obtained from a background image from pure water surface $\eta_0$. The number of thresholds that resulted in the maximum value of $\eta - \eta_0$ was selected. Thresholding performance was curated manually and images where thresholding failed were not included in the analysis. Fifth, the obtained segmented images were used as masks to calculate the area fractions and mean intensities of different film regions using the original, unprocessed images.

Fluorescence microscopy images were segmented to mono- and multilayer regions by using Otsu's method with 1–3 thresholds. Thresholding performance was observed manually and a single threshold with best performance dividing the image into monolayer and multilayer segments was selected, and area fractions of each phase were calculated.

### 2.5. Film thickness analysis

BAM images captured at mean molecular areas higher than 85 Å$^2$/POPC were included in the analysis. Average intensities were calculated from the film regions selected by using segmenting as described above. To take into account the formation of small multilayer domains below BAM resolution, which gradually increased the intensity of each segment, the lower intensity segments were discarded from the analysis in images, where more than 10% of the surface was covered by a higher intensity segment. Intensities were divided by the exposure time used when capturing the image, in order to compare relative intensities between images captured with different exposure times. Background intensity was calculated by averaging from images captured from pure water surface and subtracted from all the other measured intensities. To obtain an estimate of the relative thickness, the square root of the

intensity values was used, since for a first-order approximation, the reflectance of the surface depends on the square of the film thickness [32].

### 2.6. Evaporation resistance

Evaporation resistance was measured using the desiccant-based method proposed by Langmuir and Schaefer [33]. In short, a desiccant container with a water-permeable membrane on one side was placed for 5 min onto a custom holder within a few millimeters above the subphase surface with the membrane side facing the water surface. Based on the absorbed water mass in the presence and absence of a lipid film, the evaporation resistance was calculated as described previously [30]. Disposable desiccant cartridges (SP Industries, Warminster, PA) with silica gel were used, but the membrane was replaced with Millipore Immobilon -P PVDF membrane with 450 nm pore size (Bedford, MA).

## 3. Results and discussion

### 3.1. Multilamellar organization of cholesteryl ester:phospholipid films

To gain insight into the interplay of polar and non-polar lipids in the TFLL, we first used mixtures of POPC and CN to model the polar and non-polar parts of the TFLL, respectively. Films with varying ratios of CN and POPC were analysed using surface pressure isotherms measured on an aqueous subphase in a Langmuir trough system (see Methods). Pure CN did not form a stable film, instead liquid aggregates with colourful interference patterns were formed, as reported previously [34].

When large amounts of POPC were included in the film (3:1 POPC:CN ratios or more), CN mixed with POPC to form a monolayer at low surface pressures, as verified by the uniform intensity observed in both BAM and FM images (Fig. 2i). In the monolayer phase, CN likely adopted a kinked conformation with the ester group facing the water (Fig. 2i). As more CN molecules was added to the film, some of the CN separated to form multilayer domains on top of the monolayer, observed as high intensity domains in BAM (Fig. 2ii-iii). The multilayer structure forming on top of the monolayer has been previously termed “double layer” for unsaturated CEs with shorter acyl chains [35]. The same domains were also observed with FM, although the fluorescent Atto633-DOPE probe used resides in the polar monolayer. This effect is due to the preferential partitioning of the fluorescent Atto633-DOPE into monolayer regions that were covered by a CN layer (Supplementary Fig. 1). The regions covered by the multilayer increased with added CN, until they covered the whole film at 1:9 POPC:CN ratio (Fig. 2iv). Further increase of CN caused additional layers of CN to form on top of the first layer, but these additional layers did not spread uniformly over the film. Instead, more layers were formed locally in some areas and less in others, as observed in the BAM images (Fig. 2vi).

The multilayer domains displayed uniform intensity levels in the BAM images, which were used to estimate the relative thickness of film regions with different number of lamellae (Fig. 3A,B). A single multilayer lamella was found to be approximately three times thicker than the underlying monolayer. Considering the typical thickness of POPC monolayer hydrocarbon region (1.4 nm [36]), this would correspond to approximately 4.2 nm. This value is in line with the previous CN layer thickness estimate of 4.38 nm [34]. The multilayer domains had a round, liquid appearance, thereby indicating that the structure within the multilayer lamellae was liquid crystalline (Fig. 2iii).

The monolayer residing underneath the multilayers contained a relatively large proportion of CN at zero surface pressure (up to 30%). Upon compression of the films to higher surface pressures, CN was transferred from the monolayer into the overlying multilayers (Fig. 2ii, Supplementary Fig. 2). At surface pressures corresponding to the natural tear fluid (27–31 mN/m [37]), CN resides almost completely in the overlying multilayers.

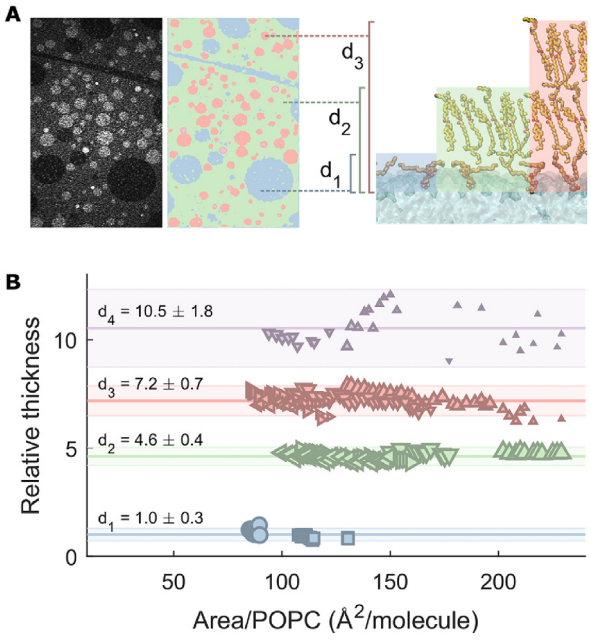


**Fig. 3.** The thickness of POPC:CN multilayer lamellae. **A)** Schematic representation of the measured relative thicknesses ($d_i$). Images were first segmented into intensity regions (shown in red, green, and blue) and the relative thickness was determined by comparing BAM image intensities of the different regions. **B)** The relative thickness of different film regions (mean ± standard deviation) compared to a monolayer ($d_1$). $d_2$–$d_4$ correspond to regions containing 1–3 overlying CN multilayers. Different symbols represent the POPC:CN ratio, ▲ = 1:9, ▼ = 1:6, ► = 1:4, ◄ = 1:3, ■ = 3:1, ● = pure POPC. Symbol size represents the area fraction of the intensity region.

As CN was transferred to the multilayers and the multilayer was compressed, the multilayer volume (per unit area) increased (Fig. 4A,B), whereas the coverage, i.e. the area fraction of the film covered by at least one multilayer lamella initially increased (Fig. 4C). However, as a surface pressure of approximately 12 mN/m was reached, the multilayer coverage started to decrease across the studied POPC:CN ranges (Fig. 4C), observed as an expansion of dark regions in the BAM and FM images (Supplementary Fig. 3), even in films completely covered by CN multilayers (Fig. 2iv-v). This indicated that CN was gradually expelled from the monolayer surface into thick aggregates, and most of the water surface was covered by only a POPC monolayer at high surface pressures (Supplementary Fig. 1). In the surface pressure isotherms, this is seen as the coalescence of POPC:CN mixture isotherms with the isotherm of pure POPC (Fig. 2).

In conclusion, these results highlight the important role that the small quantities of polar lipids have in the organization of TFLL, and provide support for the multilamellar TFLL model [15,16]. When 90% or more of the film consisted of CN and surface pressure was low (< 12 mN/m), a continuous non-polar multilayer resided on top of the polar lipid monolayer at the aqueous interface. Furthermore, compression and expansion of the layer led to production and removal of further CN multilayer lamellae. However, at higher surface pressures, corresponding to the natural tear fluid, CN did not form a uniform multilayer. Instead, thick multilamellar aggregates formed locally. Such incomplete spreading of non-polar lipids is often considered to result from a lowered concentration of polar lipids. However, as shown here, a high surface concentration of phospholipids results in the loss of non-polar lipid spreading.

To explain the loss of multilayer spreading at high surface pressures, we propose that the driving force for the formation of a uniform multilayer is the interdigitation of acyl chains between the monolayer and the overlying multilayer. This resembles the interdigitation that occurs

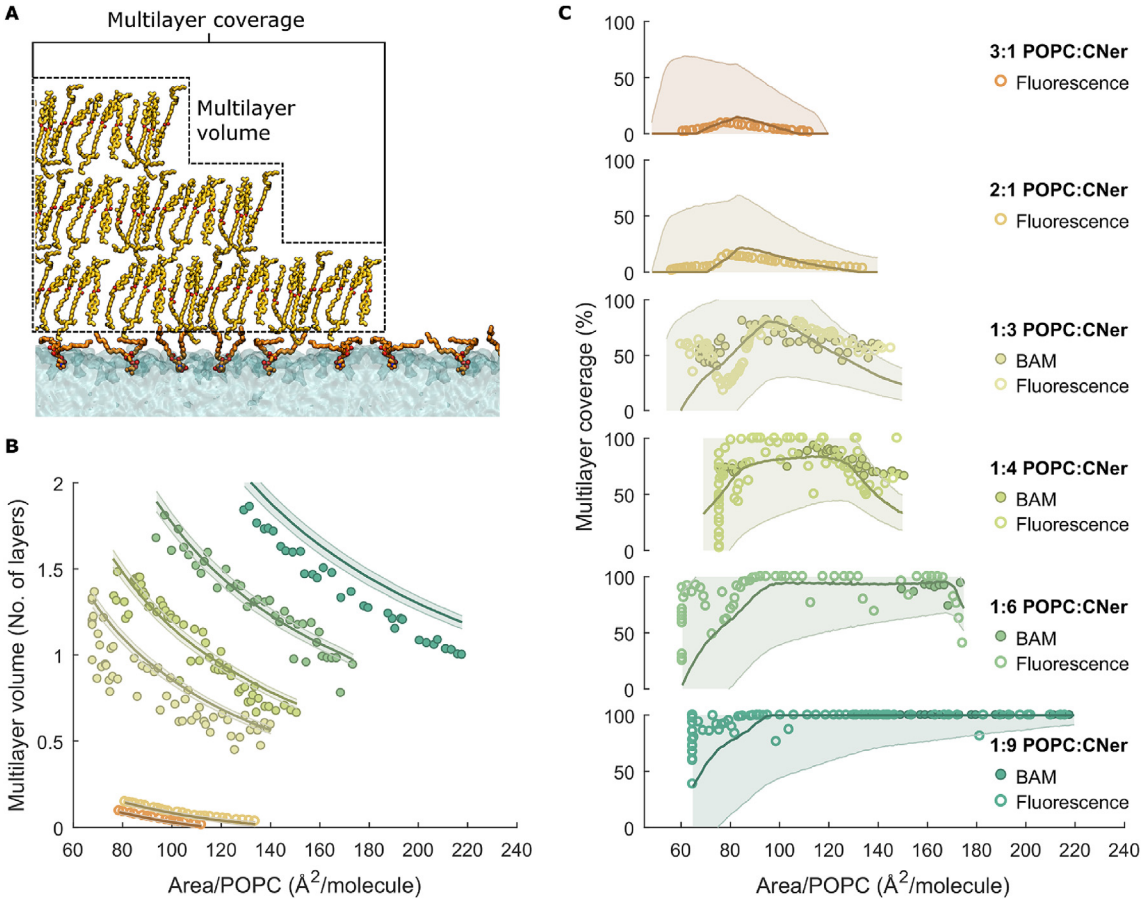


**Fig. 4.** Imaging of POPC:CN multilayer structure. **A)** Schematic representation of the measured multilayer coverage and multilayer volume. These parameters were determined from segmented BAM and FM images. **B)** Multilayer volume as a function of mean molecular area per POPC molecule. Symbols correspond to the film compositions and methods represented in panel C. **C)** Multilayer coverage as a function of POPC mean molecular area with various POPC:CN ratios. Solid lines depict the fitted model described in the text and Supplementary methods and the shaded regions depict 95% confidence intervals.

between neighbouring cholesteryl ester lamellae in bulk [38]. The interdigitation of CN acyl chains into the monolayer contributes to the entropic repulsion between neighbouring lipids in the monolayer and increases the surface pressure (Fig. 5A). To study this phenomenon, we used a model in which each CN molecule in the multilayer directly overlying the monolayer increased the total area of the monolayer by $a'_{ID}$ at any surface pressure $\pi$ (see Supplementary methods for details).

By fitting the model to the total multilayer volume shown in Fig. 4B, the area occupied by a single CN molecule in the multilayer phase ($a'_{multi}$) was estimated to be 30 ± 1 Å$^2$. This suggests that the CN multilayers have a smectic liquid crystal-like organization with antiparallel arrangement of the cholesteryl esters (Fig. 5A). This arrangement would be similar to the predominant crystal phase of CN (monolayer type II) [38], which has a mean molecular area of 28.5 Å$^2$ [39]. However, the proposed arrangement is in contrast with an earlier estimate of 38 Å$^2$ for cholesterol myristoleate multilayers, which suggested a ring-ring packing limited by the size of the cholesteryl moiety [35].

Further, by fitting the model to the multilayer coverage (Fig. 4C) we could determine the mean area of interdigitation per CN molecule in the multilayer phase, $a'_{ID}$, which contributes to the observed surface pressure (Fig. 5B). At near zero surface pressure, the area of interdigitation was estimated to be approximately 10 Å$^2$/molecule. Considering the antiparallel organization in the multilayers, only half of the CN acyl chains are oriented towards the monolayer. Therefore, each CN acyl chain would occupy approximately 20 Å$^2$ in the monolayer, suggesting that most of the acyl chains facing the monolayer are interdigitated with the monolayer acyl chains (Fig. 5i). As the surface pressure increases, the monolayer acyl chains become increasingly ordered, pushing CN acyl chains away from the monolayer as the area of interdigitation decreases to approximately 5 Å$^2$/molecule (Fig. 5ii). At this point, the cohesive interactions between CN molecules overcome the attractive interactions between the mono- and multilayer molecules, resulting in transfer of CN from the multilayer directly on top of the monolayer into overlying lamellae. This corresponds to the transition observed at 12 mN/m surface pressure, where multilayer coverage begins to decrease (Fig. 2v and 4C).

Since the interdigitation only affects the multilayer lamella adjacent to the monolayer, this mechanism also explains why further lamellae do not form in a uniform manner after the first lamella (Fig. 2vi).

### 3.2. Crystalline monolayer formation in O-acyl-hydroxy fatty acid multilayers

After discovering that an interfacial phospholipid monolayer did not support the formation of a uniform CN multilayer at surface pressures relevant to the tear film, we turned our attention to OAHFAs. OAHFAs are an unusual lipid class found in the tear film [40], which have been the subject of increasing interest after their identification. Since they are the main polar lipid class in the Meibomian gland secretions that make up the TFLL [10,21,22], they have been proposed to form the polar sublayer of the TFLL. We used an in-house synthesised (*O*-oleoyl)-ω-hydroxy arachidic acid (20-OAHFA) to represent tear fluid OAHFAs.

In mixed films of 20-OAHFA and CN, multilayer domains of CN formed over the 20-OAHFA monolayer at low surface pressures (< 2 mN/m), similar to POPC:CN films (Fig. 6i). When six or more CN

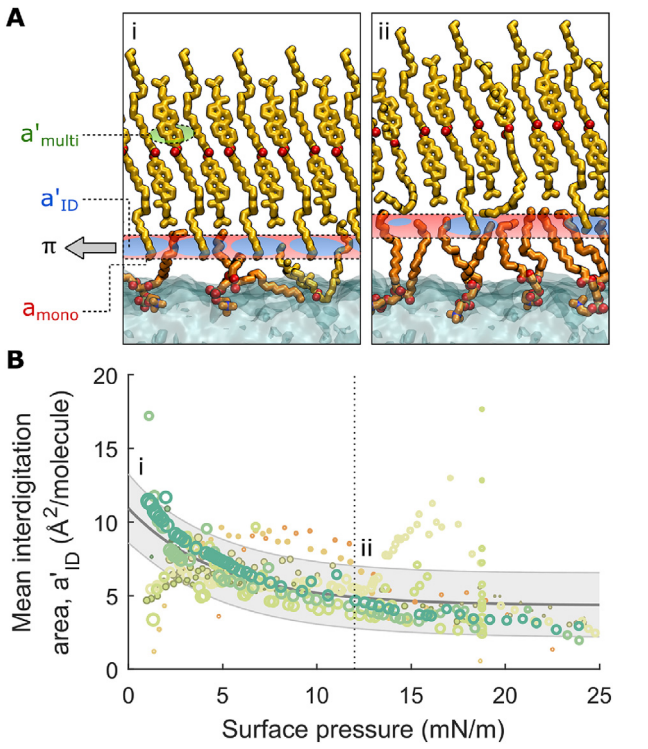


**Fig. 5.** Interdigitation of acyl chains between the monolayer and multilayer phases. **A)** Schematic representation of the molecular organization at low (i) and high (ii) surface pressures and the model parameters used in the interdigitation model. The plane depicts the region where entropic repulsion of acyl chains occurs, causing surface pressure (π). Red and blue areas represent the area contributions from the mono- and multilayer sides, respectively. **B)** Mean area of interdigitation ($a'_{ID}$) by CN in the multilayer phase as a function of surface pressure. The dashed line represents the transition pressure for the exclusion of the multilayer from the monolayer surface. Symbols represent experimental values determined from the isotherm and area fraction data (see Supplementary methods), and the solid line is an exponential fit to the data with 95% confidence interval shown. Symbol colours correspond to the mixtures listed in Fig. 4C and symbol size represents the reciprocal of the error estimate for each data point (bigger symbol = smaller error).

molecules per 20-OAHFA were included in the film, the 20-OAHFA monolayer was completely covered by a CN multilayer (Fig. 6iv). These films exhibited more complex behaviour than POPC:CN films. This is due to the liquid to solid monolayer phase transition [30], which is observed as a pronounced plateau in the isotherm of pure 20-OAHFA (Fig. 6). Therefore, in addition to the collapse of the CN multilayers observed in POPC:CN films, 20-OAHFA:CN films also exhibited a liquid-solid transition in the underlying monolayer during compression of the films. This transition was observed as growth of dark crystallites in the FM images (Fig. 6i,ii). Interestingly, the 20-OAHFA crystallites preferentially formed at the boundaries of round CN multilayer domains (Fig. 6i), likely driven by line tension of the multilayer domains and solid 20-OAHFA monolayer domains. Aside from the nucleation of 20-OAHFA monolayer crystals at the multilayer domain boundary, the surface monolayer was unaffected by the presence of an overlying multilayer and underwent a liquid-solid transition similar to a pure monolayer of 20-OAHFA (Fig. 6i,ii). This was evidenced by the liquid-solid transitions of the monolayer occurring at areas of 120–150 Å$^2$/20-OAHFA regardless of the film composition. In addition, the surface potential values of mixed films were identical to pure 20-OAHFA (Supplementary Fig. 4).

While the monolayer underwent crystallization upon compression, the overlying multilayer domains coalesced, until they covered all the monolayer regions in the liquid phase (Fig. 6ii,v). This transition occurred at an almost constant area of 23–25 Å$^2$/molecule at all film compositions studied, suggesting that both 20-OAHFA and CN contribute to the multilayer phase. Since the 20-OAHFA adopts an extended conformation in the solid phase (Fig. 6i–ii), it can be assumed to occupy ~20 Å$^2$ per molecule in the multilayer, whereas CN occupies 30 Å$^2$, explaining the almost constant mean molecular areas of this transition. Further compression caused the CN multilayer adjacent to the monolayer to collapse into additional layers on top of the first multilayer, observed as brighter regions in BAM images. When they formed over a liquid 20-OAHFA monolayer, the domains had circular shapes (Fig. 6v-vi). Upon crystallization of the monolayer, these additional layers formed in irregular shapes, determined by the network-like organization of solid 20-OAHFA monolayer regions (Fig. 6iii, Supplementary Fig. 5). This suggests that the multilayers are not able to spread on top of the solid 20-OAHFA monolayer regions. This is likely due to the inability of CN acyl chains to interdigitate into the solid multilayer domains. Therefore, compressing the film to high surface pressures caused CN to be expelled from the monolayer surface, similar to POPC:CN films, while the underlying monolayer became solid.

Both polar lipids, 20-OAHFA and POPC, induced the formation of a multilamellar lipid film of non-polar CN, when surface pressure was low (less than 2 and 12 mN/m, for 20-OAHFA and POPC, respectively). At surface pressures corresponding to the tear fluid (27–31 mN/m [37]), the multilayer was excluded from large parts of the surface. These findings challenge the traditional view of the TFLL, where a uniform layer of non-polar lipids covers the polar lipid monolayer at the aqueous tear surface (Fig. 1). The non-polar layer has traditionally been considered to be responsible for the evaporation resistant function of the TFLL [15]. However, unless specific interactions between polar and non-polar tear film lipids occur that were not captured by the model systems used here, it seems likely that at natural tear fluid surface pressures the non-polar lipid layer would de-wet from large regions of the polar monolayer. Therefore, it seems implausible that the non-polar lipid layer could be solely responsible for the evaporation resistant properties of the TFLL.

### *3.3. Non-polar CN multilayers do not contribute to the evaporation resistance of the TFLL*

To address the relative contributions of the polar and non-polar sublayers to the evaporation resistance, we measured the evaporation resistance of POPC:CN and 20-OAHFA:CN mixtures (Fig. 7). The mixtures contained enough CN to form 5 multilayers on a maximally compressed monolayer of each polar lipid. No evaporation resistance was detected for a CN multilayer spread by adding POPC, whereas a mixed film of 20-OAHFA and CN resisted evaporation, however, only to the same extent as a pure film of 20-OAHFA. Taken together, these results show that a CN multilayer offered no detectable resistance to evaporation of water. However, it did not disturb the formation of an evaporation resistant monolayer at the water interface by OAHFAs in the OAHFA:CN mixtures. We found that a surface concentration of 5 OAHFAs/nm$^2$ was required to obtain approximately 5 s/cm of evaporation resistance. This could result in up to 80% reduction in evaporation rate from the ocular surface, as described earlier [30]. Such a surface concentration could be reached if a 200 nm thick layer of meibum containing 3 mol% of OAHFAs [22] would spread on the tear film surface, and it is therefore plausible that such a layer could form *in vivo*. These results suggest that the polar lipid monolayer is an important factor in the evaporation resistant function of the TFLL. However, it should be noted that other non-polar TFLL lipids than CN may form evaporation resistant structures.

## 4. Conclusions

The results presented here provide important insights on the organization of the TFLL. By providing a comprehensive picture of the

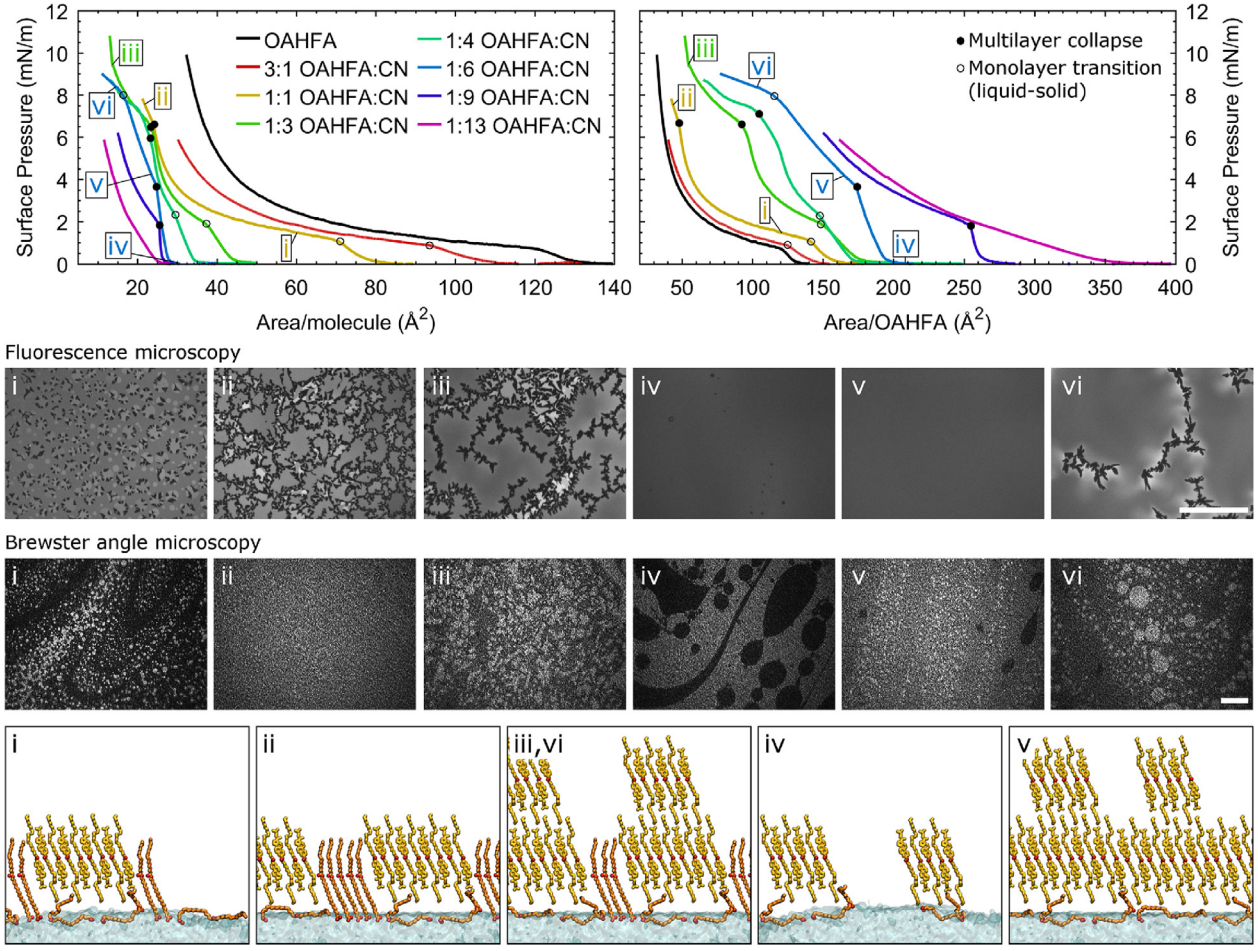


**Fig. 6.** Organization of films composed of 20-OAHFA and CN. Surface pressure isotherms of 20-OAHFA:CN mixtures with the corresponding FM and BAM images are shown, as well as a schematic representation of the film structure under different conditions (i–vi). The measurements were repeated at least twice and were found to be repeatable within 1.5 mN/m 20-OAHFAs are depicted in orange and CNs in yellow. The isotherms are presented both relative to the total number of molecules (left) and to the number of 20-OAHFA molecules (right). Scale bars represent 300 μm.

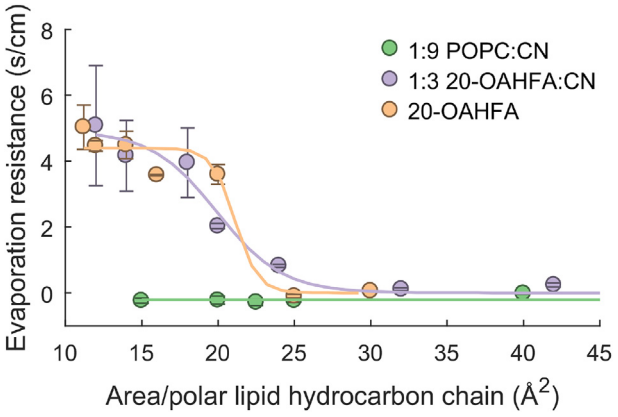


**Fig. 7.** Evaporation resistance of CN multilayer films. Films were formed by using either POPC or 20-OAHFA as the polar lipid. To facilitate comparison of different lipids, the evaporation resistance is presented as a function the area per hydrocarbon chain in the polar lipids. 20-OAHFA is considered to have a single hydrocarbon chain, where POPC has two. Each data point depicts the mean of two independent measurements and error bars show the difference between measured values. The solid lines are sigmoidal curves to fit the data.

molecular orientation in multilamellar CN films, the results elucidate the central interactions in mixed films consisting of polar lipids and non-polar lipids without inherent surface activity. Using controllable model systems, we were able to demonstrate on a molecular level, how typical patterns observed in Langmuir trough microscopy studies of meibomian and tear fluid lipid samples, such as networks of crystalline domains and multilamellar structures, can be formed. Previously, variable suggestions have been given on what these structures represent [41–44], and the results presented here provide a useful framework for interpretation of earlier findings and a solid basis for future studies on TFLL composition and function.

At low surface pressures, stable multi-layered films formed already at low surface concentrations of polar lipids (mean molecular areas of 250 Å$^2$/POPC and 350 Å$^2$/20-OAHFA). Multilayer formation appears to be driven by the interdigitation of acyl chains between the multilayer and the polar monolayer. Therefore, no more than a single multilayer lamella formed in an ordered manner. In addition, the multilayer structure was destabilized at high surface pressures due to loss of interdigitation between the layers. This has important implications for the tear film, since the surface pressure of tear fluid is relatively high. Tear fluid surface pressure is mainly due to the presence of a polar lipids, although surface active proteins may also contribute to the physiological tear fluid surface pressure [19,37]. The results of our study reveal that a stable, uniform non-polar lipid layer would not be expected to form on the surface of the tear film. Instead, certain regions would be expected to be covered by thick non-polar lipid aggregates or droplets, whereas other regions would only be covered by a monolayer. This is in accordance with clinical imaging studies, which have shown that the TFLL is not uniform on the microscale [45].

Lastly, our results provide new insights on the TFLL structure-function relationship which contrasts the commonly presented view, according to which the function of the TFLL depends on polar lipids spreading the non-polar tear film lipids on the tear film surface [15,18,46]. Our findings suggest that the spreading behaviour between the polar and non-polar layers is complex and that the CEs in the non-polar multilayers do not contribute to the evaporation resistant function of the TFLL. Instead, this attribute seems to be governed by evaporation resistant lipids, such as OAHFAs, in the polar lipid layer, which resides at the interface between the tear fluid and the non-polar lipid layer. Therefore, polar lipids appear to be central to TFLL function, whereas the function of the non-polar lipids in the TFLL is still an open question. It is possible that a part of the non-polar lipids simply act as a vehicle to deliver the more important lipids, such as OAHFAs to the tear film surface. Insufficient delivery of evaporation resistant polar lipids to the tear film surface or contamination by non-evaporation resistant polar lipids could result in loss of evaporation resistance in DES.

It should be noted that the model compositions used in this study do not perfectly match the lipid composition of the tear film. First, a most of the tear fluid phospholipids are lysophospholipids, in contrast to POPC used here. However, very similar results to those presented here were obtained also for lysophospholipids [47], and a large fraction of the lysophospholipids in the tear film are likely dissolved in the aqueous layer due their relatively high water solubility. Second, the model OAHFA used in this study (18:1/20:0) was shorter and lacked a double bond compared to the most abundant OAHFAs in the tear fluid (18:1/32:1) [10,22,48,49]. These structural differences are likely to alter the properties of the OAHFAs, but since the absence of the double bond tends to make lipid monolayers more ordered, while the shorter chain length makes them less ordered [30], these differences are likely to largely cancel each other out. Third, unsaturated CN was used to model the non-polar TFLL lipids, although a major fraction of the meibum CEs is saturated [22,50]. However, CN is still likely to reflect the physical properties of Meibomian CEs relatively well, since most of the saturated CEs in meibum are branched [51], which has a similar effect on the physical properties as unsaturation [52,53]. Finally, other non-polar lipid components, such as wax esters and diesters were not included in this study. It is possible that the presence of these lipids could lead to formation of multilayers with solid structures, as proposed by King-Smith et al. [16] Such multilayers might provide an evaporation resistant function, but the existence of such layers in the TFLL has not yet been demonstrated. Further studies addressing these topics are warranted.

## Declaration of competing interest

None.

## Acknowledgements

This work was supported by The Finnish Eye Foundation, the Mary and Georg C. Ehrnrooth Foundation, the Eye and Tissue Bank Foundation, the Evald and Hilda Nissi Foundation, Orion Research Foundation, Biomedicum Helsinki Foundation, the Neuron Endowment Fund, Czech Science Foundation (grant 18-26751S), and the state research funding in Finland. The funding sources had no role in study design, the collection, analysis and interpretation of data, writing of the report, or the decision to submit the article for publication.

## Appendix A. Supplementary data

Supplementary data to this article can be found online at https://doi.org/10.1016/j.jtos.2020.06.001.

## References

[1] Bron AJ, de Paiva CS, Chauhan SK, Bonini S, Gabison EE, Jain S, et al. TFOS DEWS II pathophysiology report. Ocul Surf 2017;15:438–510.
[2] Jones L, Downie LE, Korb D, Benitez-Del-Castillo JM, Dana R, Deng SX, et al. TFOS DEWS II management and therapy report. Ocul Surf 2017;15:575–628.
[3] Lemp MA, Crews LA, Bron AJ, Foulks GN, Sullivan BD. Distribution of aqueous-deficient and evaporative dry eye in a clinic-based patient cohort: a retrospective study. Cornea 2012;31:472–8.
[4] Nichols KK, Foulks GN, Bron AJ, Glasgow BJ, Dogru M, Tsubota K, et al. The international workshop on meibomian gland dysfunction: executive summary. Invest Ophthalmol Vis Sci 2011;52:1922–9.
[5] Nelson JD, Shimazaki J, Benitez-del-Castillo JM, Craig JP, McCulley JP, Den S, et al. The international workshop on meibomian gland dysfunction: report of the definition and classification subcommittee. Invest Ophthalmol Vis Sci 2011;52:1930–7.
[6] Arita R, Mori N, Shirakawa R, Asai K, Imanaka T, Fukano Y, et al. Meibum color and free fatty acid composition in patients with meibomian gland dysfunction. Invest Ophthalmol Vis Sci 2015;56:4403–12.
[7] Butovich IA, Wilkerson A, Bhat N, McMahon A, Yuksel S. On the pivotal role of Elovl3/ELOVL3 in meibogenesis and ocular physiology of mice. Faseb J 2019;33:10034–48.
[8] Sassa T, Tadaki M, Kiyonari H, Kihara A. Very long-chain tear film lipids produced by fatty acid elongase ELOVL1 prevent dry eye disease in mice. Faseb J 2018;32:2966–78.
[9] Miyamoto M, Sassa T, Sawai M, Kihara A. Lipid polarity gradient formed by ω-hydroxy lipids in tear film prevents dry eye disease. eLife 2020;9:e53582.
[10] Lam SM, Tong L, Duan X, Petznick A, Wenk MR, Shui G. Extensive characterization of human tear fluid collected using different techniques unravels the presence of novel lipid amphiphiles. J Lipid Res 2014;55:289–98.
[11] Lam SM, Tong L, Yong SS, Li B, Chaurasia SS, Shui G, et al. Meibum lipid composition in Asians with dry eye disease. PloS One 2011;6.
[12] Borchman D, Ramasubramanian A, Foulks GN. Human meibum cholesteryl and wax ester variability with age, sex, and meibomian gland dysfunction. Invest Ophthalmol Vis Sci 2019;60:2286–93.
[13] Chen J, Keirsey JK, Green KB, Nichols KK. Expression profiling of nonpolar lipids in meibum from patients with dry eye: a pilot study. Invest Ophthalmol Vis Sci 2017;58:2266–74.
[14] Shine WE, McCulley JP. Keratoconjunctivitis sicca associated with meibomian secretion polar lipid abnormality. Arch Ophthalmol 1998;116:849–52.
[15] McCulley JP, Shine W. A compositional based model for the tear film lipid layer. Trans Am Ophthalmol Soc 1997;95:79–93.
[16] King-Smith PE, Bailey MD, Braun RJ. Four characteristics and a model of an effective tear film lipid layer (TFLL). Ocul Surf 2013;11:236–45.
[17] Rosenfeld L, Cerretani C, Leiske DL, Toney MF, Radke CJ, Fuller GG. Structural and rheological properties of meibomian lipid. Invest Ophthalmol Vis Sci 2013;54:2720–32.
[18] Cwiklik L. Tear film lipid layer: a molecular level view. Biochim Biophys Acta Biomembr 2016;1858:2421–30.
[19] Svitova TF, Lin MC. Dynamic interfacial properties of human tear-lipid films and their interactions with model-tear proteins in vitro. Adv Colloid Interface Sci 2016;233:4–24.
[20] Georgiev GA, Eftimov P, Yokoi N. Structure-function relationship of tear film lipid layer: a contemporary perspective. Exp Eye Res 2017;163:17–28.
[21] Butovich IA. Tear film lipids. Exp Eye Res 2013;117:4–27.
[22] Brown SH, Kunnen CM, Duchoslav E, Dolla NK, Kelso MJ, Papas EB, et al. A comparison of patient matched meibum and tear lipidomes. Invest Ophthalmol Vis Sci 2013;54:7417–24.
[23] Pucker AD, Haworth KM. The presence and significance of polar meibum and tear lipids. Ocul Surf 2015;13:26–42.
[24] Leiske DL, Leiske CI, Leiske DR, Toney MF, Senchyna M, Ketelson HA, et al. Temperature-induced transitions in the structure and interfacial rheology of human meibum. Biophys J 2012;102:369–76.
[25] Leiske DL, Miller CE, Rosenfeld L, Cerretani C, Ayzner A, Lin B, et al. Molecular structure of interfacial human meibum films. Langmuir 2012;28:11858–65.
[26] Sledge S, Henry C, Borchman D, Yappert MC, Bhola R, Ramasubramanian A, et al. Human meibum age, lipid–lipid interactions and lipid saturation in meibum from infants. Int J Mol Sci 2017;18:1862.
[27] Foulks GN. The correlation between the tear film lipid layer and dry eye disease. Surv Ophthalmol 2007;52:369–74.
[28] Blackie CA, Solomon JD, Scaffidi RC, Greiner JV, Lemp MA, Korb DR. The relationship between dry eye symptoms and lipid layer thickness. Cornea 2009;28:789–94.
[29] Fenner BJ, Tong L. More to stable tears than thickness of the tear film lipid layer. Invest Ophthalmol Vis Sci 2015;56:1601.
[30] Bland HC, Moilanen JA, Ekholm FS, Paananen RO. Investigating the role of specific tear film lipids connected to dry eye syndrome: a study on O-Acyl-ω-hydroxy fatty acids and diesters. Langmuir 2019;35:3545–52.
[31] Otsu N. A threshold selection method from gray-level histograms. IEEE Transactions on Systems, Man, and Cybernetics 1979;9:62–6.
[32] de Mul MNG, Mann JA. Determination of the thickness and optical properties of a Langmuir film from the domain morphology by Brewster angle microscopy. Langmuir 1998;14:2455–66.
[33] Langmuir I, Schaefer VJ. Rates of evaporation of water through compressed monolayers on water. J Franklin Inst 1943;235:119–62.
[34] Millar TJ, King-Smith PE. Analysis of comparison of human meibomian lipid films

and mixtures with cholesteryl esters in vitro films using high resolution color microscopy. Invest Ophthalmol Vis Sci 2012;53:4710–9.
[35] Smaby JM, Brockman HL. Novel surface phase containing cholesteryl esters. 1. Structural characteristics determined from surface pressure-area measurements. Biochemistry (Mosc) 1981;20:718–23.
[36] Kučerka N, Nieh M, Katsaras J. Fluid phase lipid areas and bilayer thicknesses of commonly used phosphatidylcholines as a function of temperature. Biochim Biophys Acta Biomembr 2011;1808:2761–71.
[37] Nagyová B, Tiffany JM. Components responsible for the surface tension of human tears. Curr Eye Res 1999;19:4–11.
[38] Ginsburg GS, Atkinson D, Small DM. Physical properties of cholesteryl esters. Prog Lipid Res 1984;23:135–67.
[39] Sawzik P, Craven BM. Conformation and packing of unsaturated chains in crystals of cholesteryl nervonate at 123 K. J Lipid Res 1984;25:851–6.
[40] Butovich IA, Wojtowicz JC, Molai M. Human tear film and meibum. Very long chain wax esters and (O-acyl)-omega-hydroxy fatty acids of meibum. J Lipid Res 2009;50:2471–85.
[41] Georgiev GA, Kutsarova E, Jordanova A, Krastev R, Lalchev Z. Interactions of Meibomian gland secretion with polar lipids in Langmuir monolayers. Colloids Surf B Biointerfaces 2010;78:317–27.
[42] Millar TJ. A mechanism to explain the behaviour of spread films of meibomian lipids. Curr Eye Res 2013;38:220–3.
[43] Yoshida M, Yamaguchi M, Sato A, Tabuchi N, Kon R, Iimura K. Role of endogenous ingredients in meibum and film structures on stability of the tear film lipid layer against lateral compression. Langmuir 2019;35:8445–51.
[44] Georgiev GA, Yokoi N, Ivanova S, Tonchev V, Nencheva Y, Krastev R. Surface relaxations as a tool to distinguish the dynamic interfacial properties of films formed by normal and diseased meibomian lipids. Soft Matter 2014;10:5579–88.
[45] King-Smith PE, Nichols JJ, Braun RJ, Nichols KK. High resolution microscopy of the lipid layer of the tear film. Ocul Surf 2011;9:197–211.
[46] Rantamäki AH, Seppänen-Laakso T, Oresic M, Jauhiainen M, Holopainen JM. Human tear fluid lipidome: from composition to function. PloS One 2011;6:e19553.
[47] Paananen R, Vattulainen I, Moilanen J. Structure of tear film lipid layer models containing cholesteryl esters and lysophosphatidylcholine. Invest Ophthalmol Vis Sci 2018;59:4906.
[48] Hancock SE, Ailuri R, Marshall DL, Brown SHJ, Saville JT, Narreddula VR, et al. Mass spectrometry-directed structure elucidation and total synthesis of ultra-long chain (O-acyl)-ω-hydroxy fatty acids. J Lipid Res 2018;59:1510–8.
[49] Chen J, Nichols KK, Wilson L, Barnes S, Nichols JJ. Untargeted lipidomic analysis of human tears: a new approach for quantification of O-acyl-omega hydroxy fatty acids. Ocul Surf 2019;17:347–55.
[50] Chen J, Green KB, Nichols KK. Quantitative profiling of major neutral lipid classes in human meibum by direct infusion electrospray ionization mass spectrometry. Invest Ophthalmol Vis Sci 2013;54:5730–53.
[51] Nicolaides N, Kaitaranta JK, Rawdah TN, Macy JI, Boswell FM, Smith RE. Meibomian gland studies: comparison of steer and human lipids. Invest Ophthalmol Vis Sci 1981;20:522–36.
[52] Silvius JR, McElhaney RN. Effects of phospholipid acyl chain structure on thermotropic phase properties. 3. Phosphatidylcholines with (−), and (±)-anteiso acyl chains. Chem Phys Lipids 1980;26:67–77.
[53] Silvius JR, McElhaney RN. Effects of phospholipid acyl chain structure on physical properties: I. Isobranched phosphatidylcholines. Chem Phys Lipids 1979;24:287–96.